symmetry

Review

Discrete and Continuous Symmetries of Stratified Flows Past a Sphere

Yuli D. Chashechkin

Laboratory of Fluid Mechanics, Ishlinsky Institute for Problems in Mechanics RAS, 119526 Moscow, Russia; yulidch@gmail.com

Abstract: This study presents the detailed experimental results of fine structures and dynamics in a stratified flow past a sphere, which is towed with constant velocity in a transparent basin. We developed experimental procedures based on the complete solutions of the truncated fundamental fluid equations. These complete solutions describe the waves and fine accompanying ligaments, as well as the vortices and other flow structures. To visualize the flow, a variety of classical schlieren and electrolytic precipitation procedures were used. Ligaments appear in the schlieren images of the flow as fine interfaces and fibers. They strengthen the influence of the relatively weak density gradient in a continuously stratified fluid (CSF). The symmetry in the wake is discrete at small Froude numbers with the domination of buoyancy effects. At increased velocity and high Froude numbers, when the inertial and non-linear effects turn out to be significant, an axial symmetry becomes continuous.

Keywords: stratified fluid; towing sphere; schlieren instrument; electrolytic precipitation; internal waves; prismatic wake; vortex column; rings

Citation: Chashechkin, Y.D. Discrete and Continuous Symmetries of Stratified Flows Past a Sphere. *Symmetry* **2022**, *14*, 1278. https://doi.org/10.3390/sym14061278

Academic Editors: Andrzej Herczyński and Roberto Zenit

Received: 24 May 2022
Accepted: 13 June 2022
Published: 20 June 2022

1. Introduction

Denser particles sink, while lighter particles float under the impact of buoyancy forces. Naturally, a stratification in a heterogeneous liquid or gas occurs (a stratification is a continuous variation of density $\rho(z)$ over depth z).

The stratification is discrete when the density changes abruptly. It happens at the boundaries of immiscible media; for example, between the atmosphere and the hydrosphere.

With density changes, we observe the variations of such physical properties as the velocity of sound propagation, the refractive index of light [1]. They allow observing the patterns of flows in the bulk or on the surface of a liquid either with the naked eye [2] or using optical [3,4] and acoustic instruments [5].

The development of space technologies for remote sensing has opened up new ways for tracking the temporal variability of naturally occurring structures in the atmosphere and the oceans [6]. The received images of natural phenomena are useful for further development of the theory of fluid flows, and for the improvement of their numerical simulation and laboratory modeling.

The natural length scale $\Lambda = |d \ln \rho(z)/dz|^{-1}$, the frequency $N = \sqrt{g/\Lambda}$, or the buoyancy period $T_b = 2\pi/N$ are applied to describe the continuous stratification of incompressible liquids in environmental, industrial, or laboratory settings.

Natural oscillations of stratified media were noticed as early as the 18th century [2] and their frequency was calculated a century later [7]. There are two types of continuous stratification. Strong stratification, with $N \sim 1\ \mathrm{s}^{-1}$, is typical for laboratory conditions, and the weak one with $N \sim 0.01\ \mathrm{s}^{-1}$ characterizes the ocean and planetary atmospheres, as well as two types of uniform density fluids that are nearly homogeneous ($N \to 0 \sim 10^{-5} \neq 0$) or actually homogeneous, with $N \equiv 0$. The condition of an actually uniform density $\rho \equiv 0$ leads to the degeneration of the fundamental equations system and to a confusing of "motion" and "flow" concepts. The motion, which is considered to be a transformation of a metric space into itself, and the flow, which is a physical process of matter, momentum, and energy transfer, become mathematically undistinguishable in approximation of an actually homogeneous liquid [8].

A standard classification of flows, including laminar (layered) and irregular (turbulent) flows [9,10], is based on the characteristic structural features of flow patterns. Specific forms of phenomena at a smaller scale allow distinguishing waves and vortices [9,10]. They were visualized with a pen and brush beginning with the expressive drawings of Leonardo da Vinci and other Renaissance artists [11], and then by optical instruments [12].

Numerous experiments [12] showed that at low velocities the symmetries of homogeneous fluid flows around obstacles depend on the shape of the body even in the case of a spatially uniform flow.

The aesthetic aspect of the symmetric flow patterns influences positively the mathematical description with the reduced dimension of the problem.

Correspondingly, the solutions of classical flow problems are significantly simplified (in particular, for the flows around a sphere or a disk [9,10]). The natural flow pattern in the bulk of a homogeneous liquid does not depend on the directions of the velocity vector with respect to the gravity acceleration vector.

Surprisingly, even if the stratification is weak (i.e., the density variations on the body size can hardly be registered by modern instruments), it is noticed both in the dynamics and in the structure of the flow.

In a heterogeneous medium there are directions, with the gradients of a gravitational force potential, $\mathbf{g} = -\nabla\Phi$, determining the free-fall acceleration $\mathbf{g}$ and the density gradient $\nabla\rho$. The action of noncollinear gradients directly produces vorticity in the liquid flow [13].

The greatest gradients are placed near the surface of the submerged body, where the action of various anisotropic mechanisms of energy and matter transfer is the most pronounced. In a moving fluid the energy is transferred by macroscopic processes (by the flows with the local velocity $\mathbf{v}$ and different waves with the group velocity c_g), as well as by microscopic processes (the slow atomic–molecular diffusion as well as fast processes of direct transfer of internal energy into thin flow components [8]).

The calculations show that the stratification removes the degeneracy in the singular components of the complete solution of the linearized set of fundamental equations (i.e., the multiplicity of the dispersion equation roots for homogeneous liquids [8]).

Simultaneously, it elucidates a number of hydrodynamic paradoxes [14].

The anisotropy of the stratified media affects the redistribution of energy between the structural components in a thin layer near the surface of the submerged body. The purpose of our study is to reveal the influence of a continuous stratification on the symmetry breaking in the flow past a sphere—a perfectly symmetric body.

2. A Brief History of Flow around a Sphere Studies

There were a number of theoretical and practical reasons why scientists took interest in studying the flow around a uniformly moving sphere.

For many centuries, balls made of various materials (from natural stones to metal alloys) served as artillery shells and moveable parts in many transport mechanisms. In the middle of the 18th century, with the development of universities, the problem of flow around a sphere became the object of intensive theoretical and experimental research. The studies were carried out inquisitively, as a consequence of scientific development logic, and under government contracts in Russia [15], UK [16], Germany [17], and France [18]. The result of this research work was the creation of the continuity equation for an incompressible fluid and a compressible gas [19] and the formulation of the first closed system of equations for ideal fluid flows [20]. Paradoxical results of their application to the drag on a sphere problem were established very soon.

New energy transfer equations (for heat transfer [21]) contributed to the development of Navier's theory of fluid motion, incorporating shear stresses caused by viscous friction [22]. G.G. Stokes re-derived Navier's equations of a viscous fluid motion in terms of the continuous medium conception [23].

Analyzing the damping of oscillations of a pendulum gravimeter, he calculated the drag on a sphere in axial symmetric flow [24] in a linear approximation and created the basis of subsequent experimental and theoretical studies.

In experiments, marking impurities in the form of small immiscible liquid drops, solid particles or gas bubbles were introduced to discrete visualization of the flow pattern in a homogeneous liquid [12]. Schlieren instruments, sensitive to variations in the density gradient, were used for continuous visualization of the flow patterns in a stratified medium in addition to separated markers [4,25]. The method was chosen based on the analysis of the system of governing equations and in agreement with traditional approaches.

3. System of Stratified Fluid Mechanics Equations

The effects of compressibility and heat transfer are usually neglected in the case of slow, compared to the velocity of sound, flows of low-viscosity liquids with high heat capacity [10,26].

The equations of state for the Gibbs potential and the thermal diffusivity equation are omitted from the general system of equations as well [8]. The unperturbed (initial) density profile $\rho_0(z)$ replaces the equation of state (in a coordinate frame used further axis z is vertical and opposed to the gravity acceleration $\mathbf{g}$; the body moves along axis x).

The main physical quantities characterizing the state and flow of stratified media are density ($\rho(\mathbf{x}, t)$), momentum ($\mathbf{p} = \rho\mathbf{v}$), or velocity ($\mathbf{v} = \mathbf{p}/\rho$), defined as the ratio of invariant parameters, concentrations of the stratifying $S = S_0(z) + s$, and visualizing c components. The truncated system of equations for an incompressible stratified fluid with the linearized equation of state includes the equations of continuity, momentum transfer, diffusion for the stratifying component, and visualizing impurity, in the Boussinesq approximation, and takes the following form [8,10,26]

$$\begin{gathered}
\operatorname{div}\mathbf{v} = 0; \quad \rho = \rho_{00}\left(1 - \frac{z}{\Lambda} + s + c\right); \\
\frac{\partial \mathbf{v}}{\partial t} + \mathbf{v}(\nabla\cdot\mathbf{v}) = -\frac{1}{\rho_{00}}\nabla P + \nu\Delta\mathbf{v} - (s+c)\mathbf{g}; \\
\frac{\partial s}{\partial t} + \mathbf{v}\cdot\nabla s = \kappa_S\Delta s + \frac{v_z}{\Lambda}; \quad \frac{\partial c}{\partial t} + \mathbf{v}\cdot\nabla c = \kappa_C\Delta c.
\end{gathered} \tag{1}$$

Here, ν is the kinematic viscosity, κ_S and κ_c are stratifying agent and the impurity diffusion coefficients, ρ_{00} is the density on a reference level, and s and c are the density and impurity perturbations (contraction coefficients are included in the definition). The boundary conditions on the surface of a fixed or a uniformly moving sphere with velocity U are traditional. They are no-slip for velocity and impermeability for substances on the surface of the sphere or the surface flux for a visualizing component $j_n = j_c$ [8,27].

System (1) is characterized by a set of physical parameters, transforming into a number of temporal and spatial scales. The density profile defines the scale of stratification Λ. The ratio of a sphere diameter D to velocity U forms the kinematic time scale $\tau_D = D/U$. The attached internal wavelength is $\lambda= UT_b$.

Kinetic coefficients determine a relatively large viscous wave scale $L_N^\nu = \sqrt[3]{g\nu}/N$ as well as a fine scale $L_g^\nu = \sqrt[3]{\nu^2/g}$ and transverse scales of the ligaments due to viscosity $\delta_N^\nu = \sqrt{\nu/N}$ or diffusivity of the stratifying $\delta_N^{\kappa_s} = \sqrt{\kappa_s/N}$ and of the visualizing impurity $\delta_N^{\kappa_c} = \sqrt{\kappa_c/N}$.

The thicknesses of an additional group of ligaments depend directly on the body velocity $\delta_U^\nu = \nu/U$, $\delta_U^{\kappa_s} = \kappa_s/U$, $\delta_U^{\kappa_c} = \kappa_c/U$ [8,27]. The dynamics of the fine components is characterized by a small intrinsic time scale, $\tau_U^\nu = \delta_U^\nu/U$, reflecting a possible ability of fast rearrangement of the flow pattern. A large number of small scales (for laboratory conditions $\delta_N^\nu \sim \delta_\omega^\nu \sim 1$ mm, $\delta_N^\kappa \sim 0.05$ mm, $\delta_U^\nu \sim$0.1 mm for $N \sim 1$ s^{-1}, kinematic viscosity $\nu = 0.01$ cm^2/s, and a table salt diffusion coefficient $\kappa \sim 1.4 \cdot 10^{-5}$ cm^2/s) show the complexity of the fine structures of stratified flows. It requires their investigation methods and instruments with a high temporal and spatial resolution.

Ratios of scales define the traditional dimensionless combinations, which are the Reynolds number, $\mathrm{Re} = D/\delta_U^\nu = UD/\nu$ (and its analogues—Peclet number with diffusion coefficients $\mathrm{Pe} = UD/\kappa$); Froude number, $\mathrm{Fr} = (\lambda/2\pi D)^2 = (U/ND)^2$, equaling the reciprocal value of the energetic criterion; Richardson number, $\mathrm{Ri} = \omega_U^2/N^2$, $\omega_U = (\partial U/\partial z)$, which is widely used in the theory of stratified turbulent flows [28]; a large length scale ratio, $\mathrm{C} = \Lambda/D$; Schmidt number, $\mathrm{Sc} = \nu/\kappa_s$; and others not so frequently used.

The classification of flow components is based on a complete solution of the linearized system (1), followed from implementations of the compatibility condition [29]. It includes waves and supplementary ligaments.

Internal waves in the bulk of a CSF are visualized by schlieren instruments [4,25]. Registered variations in the magnitude and gradient of the optical refractive index illustrate the displacements of fluid particles from equilibrium positions [30].

The schlieren images of the internal waves coincide with the calculations based on the linear theory of the amplitude-phase properties of the attached waves. These waves are created by a horizontally moving sphere and along an inclined trajectory [31–33].

Ligaments are described by the singular components of the complete solutions of fundamental equations system [8,10,26] and its reduced version (1). They correspond to thin high-gradient interfaces and fibers in the wake past an obstacle [34]. A special class of fine flows (diffusion-induced flows (DiF)) is formed due to the inhomogeneity of the molecular transfer of the stratifying component and interruption of the transfer on the impermeable surface of a rigid body. We can observe them near a motionless body in a fluid at rest [9,35], but when the motion starts, DiF transform into fine disturbances. These fine disturbances in the vicinity of a moving body are drawn out by the shear flow as interfaces and filaments in the wake. They are extended by the mean flow and slowly widened under the action of molecular processes [36].

The formation of each structural component, which is the wake as a whole, vortices, and internal waves, as well as the general and fine deformation of the density profile, contributes to the drag force. A relatively small contribution of wave effects to a total drag coefficient at large values of the Froude number increases with a decreasing sphere velocity, reaching the maximum in the interval $0.7 < \mathrm{Fr} < 1$ or $4.4 < (\lambda/D) < 6.3$ [31,37,38] and decreases further when the body velocity grows. It follows from the theory of linear internal waves. Moreover, the results agree with measurements [37–40]. Additional simplifications, including the assumption of the absence of diffusion $\kappa_S = 0$ [41] or the equality of dissipative coefficients of kinematic viscosity and diffusivity $\mathrm{Sc} = \nu/\kappa_S = 1$ [42], are made when constructing the numerical solutions of a complex multiscale system (1).

The system (1) turns into the classical Navier–Stokes equations with the approximation of an actually constant density, in which the diffusion equations and the term with the force of gravity in the momentum transfer equation are excluded [10]. The patterns of pressure fields, velocity, and vorticity components determine the laminar or turbulent nature of the flow. The detailed calculations of the streamlines, pressure, and the vorticity fields in the wake past the sphere in the mode of a toroidal rear vortex formation, as well as the shape and position of the separation line, were carried out [43].The determination of the position of singular points on the flow separation line and the classification of the shapes of vortex elements in the wake supplement the calculations of forces acting on the sphere [44]. The calculated flow pattern past the sphere in the range $20 < \mathrm{Re} < 400$ gave the angular position of the circular separation line of the wake with the vortex structure [45].

Fine visualization of the vortex structure of the axisymmetric dyed wake past the sphere at low Reynolds numbers (the soluble dye was washed off the surface of a freely falling body) helps register the attached rear toroidal vortex outer shape. Its axisymmetric envelope gradually changes from a concave form into a conical and convex forms with an increasing velocity [46]. Comparison with the previous experiments shows that the rear vortex exists at Re $\sim$ 10 and even lower values of velocity Re $\approx$ 3.5.

Difficulties in studying flows with low body velocities are associated with uncontrolled background fluid motions. They occur because of the temperature or atmospheric pressure variations and mechanical movements of the basin excited by street traffic. For the visualization of the liquid flow pattern around a sphere, a soluble dye as well as luminescent compositions have been applied, which glow brightly in ultraviolet light, highlighting hydrogen bubbles and small particles. These small particles allow the recording of the flow velocity and flow patterns with 2D and 3D PIV tools.

Oil slicks, smoke, small particles, drops, and silk threads are used in wind tunnels in approximation that the impurity is "passive"; i.e., it is completely carried by the flow. However, this assumption should be confirmed in each specific case, taking into account the difference in the molecular properties of the studied and visualizing media, the Brownian motion of small particles, as well as the transfer and rotation of free solids in the shear flow.

At high velocities, when compressibility effects are evident, the schlieren instrument [3,4] becomes the most effective tool for the visualization of a general flow pattern and singular fine components such as shock waves, wake envelopes, sharp interfaces, and thin fibers (ligaments), which transfer energy, momentum, and density perturbations from the body boundary into shock waves and the wake [47,48].

4. Visualization of a Stratified Flow around a Sphere

The study of the stratification effects is usually carried out in a transparent basin filled with a sodium chloride solution of variable concentration using the "continuous displacement" method [49,50]. The linear relationship of background density and the optical refractive index [51] allow the application of various optical imaging methods, which accompany the techniques for homogeneous media [3,4,12]. The direct shadow and various versions of the schlieren methods, both the classical ones with a slit diaphragm and the Foucault knife [3,4,51,52] and technically more simple "synthetic" or moiré schlieren methods, have been applied to the study of stratified flows [53,54]. Although classical schlieren instruments have a higher sensitivity and spatial resolution than moiré tools, in practice the latter have become more widespread due to the consistency with modern PC image processing.

The high chemical activity of the NaCl solution was used for visualization in an "electrolytic precipitation" method; i.e., electrochemical anodic oxidation of lead, tin, or their alloys under the action of direct electric current [55,56]. Small particles of metal oxides and chlorates with a size of about one micrometer, formed as a result of a complex of chemical reactions, produce a white translucent suspension. The shape and location of the electrodes determine the position of the source and the density of the suspension The flow pattern resembles the tinting of flows with smoke or microdrops in wind tunnels and soluble dyes in the aquatic environment [12].

In the process of studying the effect of stratification on the flow pattern around a sphere, we mainly paid attention to the description of internal waves, which caused the displacements of fluid particles from equilibrium positions [30,31] as well as high gradient interfaces and fibrous. Fine flow components characterizing ligaments were not identified by most of the traditional imaging methods [12], including moiré or "synthetic schlieren" methods [53,54], nor suspended particles, because of the limited spatial and temporal resolution (the impact of temporal resolution importance was illustrated in [12] as well).

5. Laboratory Experiment Technique

The studies of the flow patterns around a sphere towed in a CSF or homogeneous fluid were carried out on the setups "Wave Fields Fine Structure Modeling (WFF) and "Laboratory Mobile Tank (LMT)", as a part of the Unique Science Facility "Hydrophysical Complex of the IPMech RAS". This complex was used for the modeling of hydrodynamic processes in the environment, their impact on underwater technical objects, as well as the distribution of impurities in the ocean and atmosphere (USF HPC IPMech) [57]. The setups differ in the size of the working basins ($0.7 \times 0.25 \times 0.7$ m^3 for WFF and $2.20 \times 0.40 \times 0.60$ m^3 for LMT) and a number of auxiliary mechanisms. A photo of the WFF setup is shown in Figure 1; a detailed description of the LMT setup is given in [28]. The models are towed by one movable or two thin threads (tight, stabilizing the trajectory, and a towing wire) with constant and variable velocities. Schlieren images of the flows were produced by the IAB-458 instrument (a field view is 23 cm).

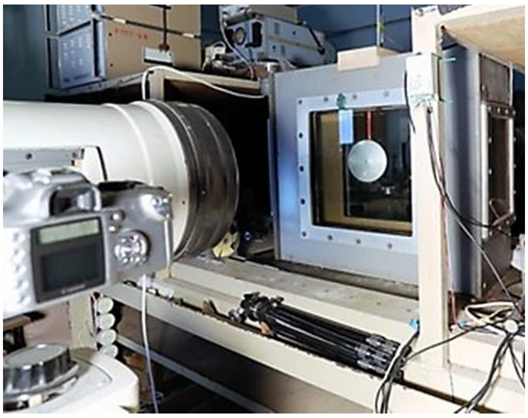

Figure 1. Experimental setup WFF USF of the "HPC IPMech RAS".

The basin was filled with an aqueous solution of common salt of variable concentration with a selected density profile by the continuous displacement method [49,50]. Flow patterns were observed around a sphere made of Plexiglas with a diameter of D =1, 2, 3, 4, 5 cm, which was placed ($U = 0$) in the tank or towed at a constant velocity U. A tin belt or segment was placed on some sphere surfaces (Figure 2). Formed particles from monoxide and oxide of tin, tin dichloride, and tin acids with a size of about 1 µm under the action of a direct electric current were transported by the flow. When the electric current increased, the larger particles were formed and the wake containing them began to sink as a whole, which was especially noticeable in a homogeneous liquid. The surface of the sphere was carefully polished before each experiment and the traces of the metal oxidation were removed.

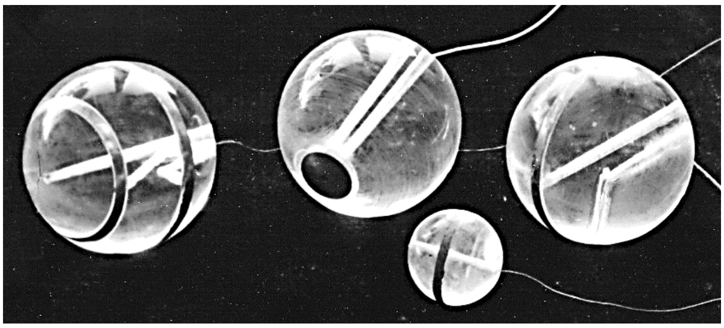

Figure 2. Spheres with anodes of various shapes.

The main stratification parameter, the buoyancy period T_b, was measured with an optical instrument [58] or an electrical conductivity sensor [59] in a short internal wave field around a density marker—a vertical wake past a rising gas bubble or a sinking crystal (salt or sugar). The bubble floated (the crystal sank) vertically if the Reynolds number, determined by its diameter D and velocity U, satisfied the condition $\mathrm{Re} = UD/\nu < 201$. In these experiments, the buoyancy period was in the range $3.5 < T_b < 14$ s.

A vertical slit was installed in the illumination part of the IAB-458, and a Foucault knife or Maksutov's thread was placed in the receiving part of the instrument to visualize the fields of the horizontal component of the refractive index and density gradient, respectively. A colored schlieren method ("natural rainbow" schlieren [52]) with a horizontal slit and a linear grating in the receiving part visualized the vertical component of the refractive index gradient. With auxiliary optics, the spatial resolution of the instrument was better than 0.01 cm.

6. Laboratory Studies of Stratified Flows

The center of mass of the stratified fluid layer is located below the geometric center in the gravity field. It means that a non-equilibrium medium with the density profile has supplies of available potential energy. The latent energy is converted into the kinetic energy of the liquid flow in a thin layer of DiF near an inclined impermeable surface, on which the molecular transfer of the stratifying component is interrupted. There is flow if the gravity field is formed, even in the absence of additional external forcing. The nature of such flows is the difference between atomic–molecular interactions in the bulk of a liquid and near a solid body boundary. The mechanism of fine flow structure formation by interruption of the diffusion flux is universal and exists in all types of non-uniform density liquid and gas flows. Firstly, the theory of stationary DiF on an infinite inclined plane was developed [9,35]. The profiles of salinity and velocity of this stationary flow are similar and characterized by a common combination scale, $\delta = \sqrt[4]{\nu\kappa_S/N^2\sin^2\alpha}$, where α is the inclination angle of the plane to the horizon. The solution diverges at small values of the angle α of plane inclination.

The salinity and velocity perturbation profiles are characterized by different transverse length scales for salinity and velocity perturbations in asymptotic solutions for small-time approximation, presented firstly in [60] and in first terms of the exact solution expansions constructed in [61].

In the local coordinate frame (ξ, ζ), axis ζ is normal to the plane; the asymptotic solution in the small-time approximation for salinity perturbations is characterized by the length scale $\delta_N^{\kappa_S} = \sqrt{\kappa_S/N}$, where time t is normalized by the buoyancy period $\tau = t/T_b$ [60],

$$s' = -2\frac{\delta_N^{\kappa_S}\sqrt{\tau}}{\Lambda}\mathrm{ierfc}\left(\frac{\zeta}{2\delta_N^{\kappa_S}\sqrt{\tau}}\right), \tag{2}$$

The asymptotic expression for the velocity of the induced velocity is described by both scales $\delta_N^{\kappa_S}$ $\delta_N^{\nu} = \sqrt{\nu/N}$ [60],

$$\begin{gathered} u(\zeta) = \frac{N^2\ \delta_s\ \tau^{3/2}}{\nu-\kappa_s}\left[\mathrm{i}^3\mathrm{erfc}\left(\frac{\zeta}{2\delta_\nu\sqrt{\tau}}\right) - \mathrm{i}^3\mathrm{erfc}\left(\frac{\zeta}{2\delta_s\sqrt{\tau}}\right)\right]\sin 2\alpha, \\ \mathrm{i}^n\mathrm{erfc}(z) = \int_z^\infty \mathrm{i}^{n-1}\mathrm{erfc}(x)dx,\ \mathrm{i}^0\mathrm{erfc}(z) = \frac{2}{\sqrt{\pi}}\int_z^\infty e^{-x^2}dx,\ \mathrm{i}^{-1}\mathrm{erfc}(z) = \frac{2}{\sqrt{\pi}}e^{-z^2}. \end{gathered} \tag{3}$$

The flow components with incommensurable length scale values show the total unsteadiness of the phenomena.

The flow pattern consists of a sequence of counter flows with rapidly decaying amplitude. Due to the smallness of the transverse scales, it does not practically depend on the shape of the body everywhere, except for its poles, which are the extreme points of the obstacle in the vertical plane [62]. Thin DiF are not resolved by the mostly used methods of a flow visualization.

The geometry of the problem and the consistency of the diffusion flux on the overhanging surface (an excess of salt accumulates on this surface) form a directed downward flow.

The flow is directed upward on an open inclined surface where a salt deficit is observed. Accordingly, the flow around the sphere is symmetric with respect to the vertical axis and is antisymmetric with respect to the plane of the horizontal equator. Asymptotic and numerical solutions of the system (1) for DiF on a sphere are presented in [63].

Here, the sections of the sequence of emerging toroidal vortices, which form convergent and divergent jets near the upper pole of the sphere, are shown in Figure 3. Amplitudes of perturbations rapidly decay with distance from the body surface.

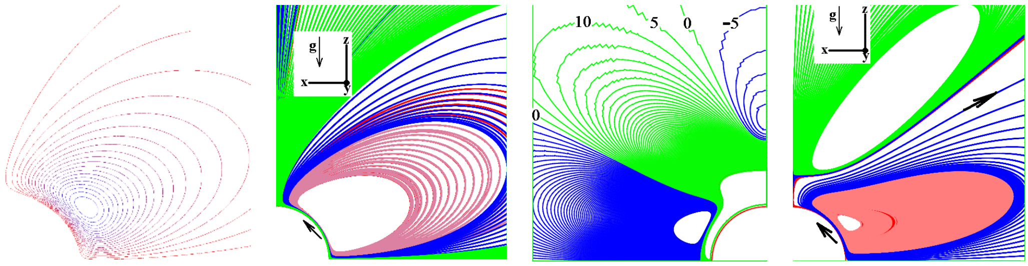

(**a**) (**b**) (**c**) (**d**)

Figure 3. Pattern of the DiF flow on a fixed sphere of a small diameter (d = 2 cm, T_b = 6.34 s): (**a**,**b**)—streamlines from the analytical solution and numerical simulation t = 0.5 T_b; (**c**,**d**)—salinity disturbance isolines and streamlines, $t = T_b$.

The results of the numerical and analytical solution of the system (1) agree quite well. In the non-stationary pose, new circular cells appear subsequently near the pole of the sphere with a buoyancy period. Each new cell shifts the entire system of perturbations that have arisen earlier onto the sphere surface. The general shape of the flow structure does not depend on the size of the sphere; however, the thickness of the cells and the flow velocity increase with the growth of the body diameter.

The comparison of calculations of the flow pattern at short and long times (Figures 3 and 4) shows that the number of cells, as well as the value of the maximum velocity, steadily increases, and the rate of change gradually fades. However, the flow does not have a stationary limit. The free symmetric body remains motionless on the horizon of neutral buoyancy due to the geometry of the flow.

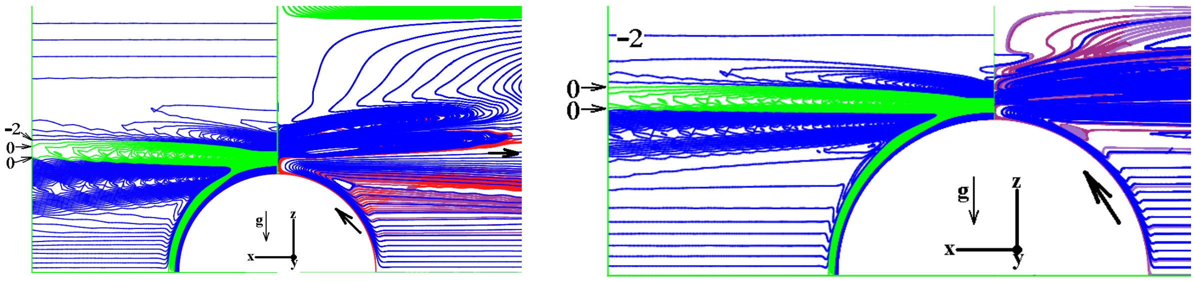

(**a**) (**b**)

Figure 4. Central section of a DiF pattern on the upper half of the sphere (T_b = 6.34 s): (**a**,**b**)—D = 2, 4 cm, $\tau = t/T_b$ = 1662, 1075; there are salinity disturbances on the left side of the figures, and streamlines on the right side (image scales are different).

In the schlieren photographs of the flow around a motionless sphere, the symmetrical pattern contains a sequence of widening dark and light bands near the poles. The angle of inclination of the bands to the horizon monotonically decreases with distance from the source (Figure 5a,b). The shape of the flow near the poles of a sphere, which indicates a noticeable change in the density gradient in a thin layer, is in good agreement with the calculation [63]. A geometrically similar flow is located at the edge of a cell of thermoconcentration convection over a localized ("point") heat source in a CSF. It was interpreted as "dissipative-gravitational waves" in [64].

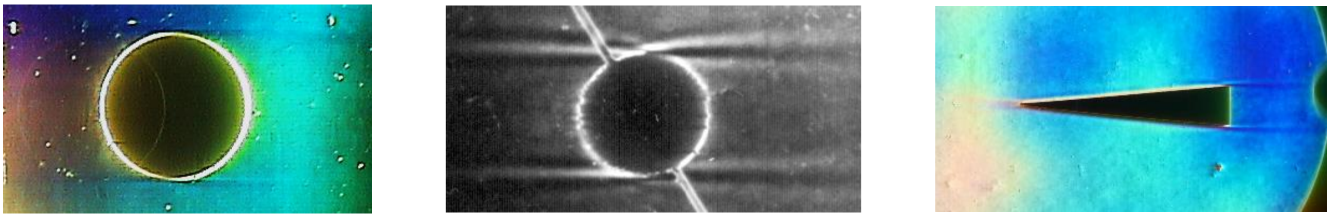

(**a**) (**b**) (**c**)

Figure 5. Schlieren pattern of DiF, $T_b = 6$ s: (**a**,**b**)—on a sphere $D = 5$ cm (Maksutov's thread and Foucault knife), and (**c**) on a wedge of length L = 10 cm and the base height h = 2 cm suspended on the horizon of neutral buoyancy.

A general change in the density distribution influences the molecular diffusion in the flow fluid near the inclined surface of an impermeable body. The intensification of the density gradient in an almost resting liquid confirms the non-stationarity and spatial inhomogeneity of the process of a flow formation. It transforms a weak mean gradient into a stronger one in the thin layer. Numerical calculations of the DiF were carried out on the basis of the system of Equation (1) near various bodies that are an inclined plate [62], a sphere [63], or a horizontal wedge [65–67].

DiF transport the substance along the side faces of the wedge and creates a deficit of mass ahead of the apex. The asymmetric distribution of pressure in the flow pattern induced by diffusion on a motionless wedge includes the area of pressure deficit in front of its apex (Figure 6a). It causes self-motion of the asymmetric body [65,66].

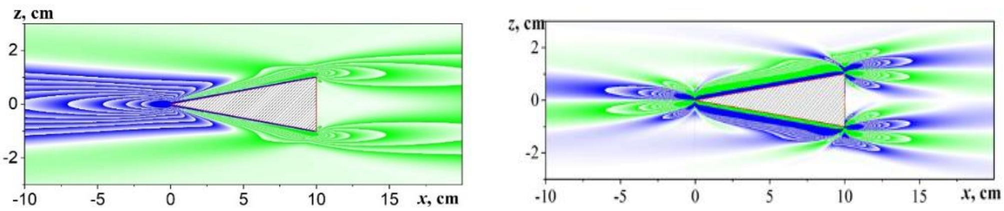

(**a**) (**b**)

Figure 6. Calculated DiF pattern near a fixed wedge (length L = 10 cm, shelf height h = 2 cm) in CSF at rest, $T_b = 6.3$ s: (**a**,**b**)—disturbances of the pressure and the horizontal component of the density gradient.

The fact that the height of the pressure deficit area even somewhat exceeds the height of the body base, ensures the efficiency of its action. In this case, the variations in velocity, salinity, and the horizontal component of its gradient are concentrated in thin layers adjacent to the lateral surface of the wedge (Figure 6b).

In the experiment, the interfaces are weakly expressed ahead of the body apex and are distinctly expressed at the edges of the base, as is shown in the schlieren image of the flow in Figure 5c. The self-motion of a wedge is experimentally demonstrated in [65,67]; a detailed calculation and schlieren visualization of the flow pattern is given in [66].

7. Rectangular Cross-Section of the Density Wake Past a Sphere at Low Froude Number

As the sphere starts to move in the horizontal plane, the pattern of DiF as a whole and its symmetry changes radically. To visualize the fine structure of the wake past the sphere and its spatial shape we used sensitive schlieren methods and electrolytic precipitation.

Careful examination of the images in Figure 7 shows that the axisymmetric DiF near the poles of the sphere is transformed into unsteady upstream internal waves that are continuations of the attached waves past and above the sphere. Ligaments correspond to extended double light/dark stripes adjoining the poles past the sphere in Figure 7a,c [8].

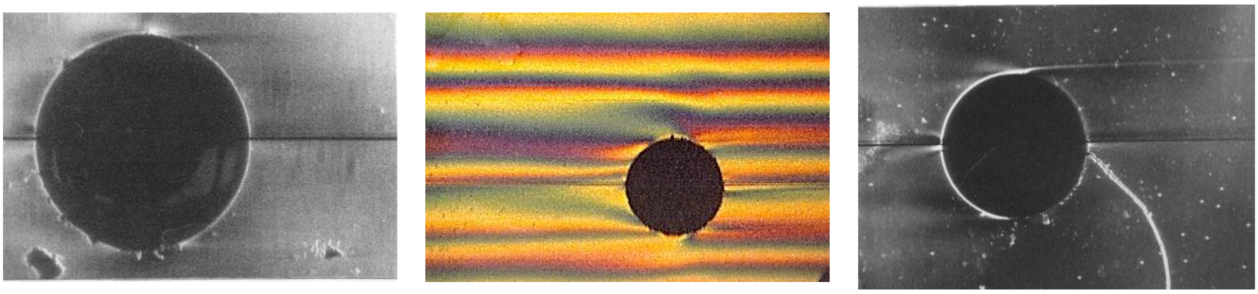

(**a**) (**b**) (**c**)

Figure 7. Schlieren images of the flow around a sphere moving slowly from right to left in CSF: (**a**,**b**)—$T_b = 8.0$ s, $N = 0.785$ s^{-1}, $D = 4$ cm, $U = 0.04$; 0.06 cm/c, $\mathrm{Fr} = U^2/N^2D^2 = 1.6 \times 10^{-4}$, Re = 16; 24, conventional and natural rainbow schlieren methods; (**c**)—$T_b = 4.5$ s, $N = 1.4$ s^{-1}, $D = 5$ cm, $U = 0.08$ cm/s, Re = 40, Fr = 1.3×10^{-4} (vertical slit—Foucault knife).

DiF are transformed into the inclined beams of non-stationary internal waves, which are oriented in the direction of the sphere motion in front of the body. Light bands near the upper and the lower poles ahead of the sphere in Figure 7a,c, outline the blocked fluid moving together with the body. The blocked fluid is characterized with a more uniform density profile than the initial one. The boundaries of the blocking zone are better expressed in the color schlieren image of the flow in Figure 7b ("natural rainbow" method). Here they are represented by an inclined blue strip, extending from the lower pole of the sphere and pale from the upper pole, oriented in the direction of the body's velocity; it is converging with distance.

Contractions and expansions of the colored bands in a schlieren image of above the sphere flow (Figure 7b) visualize the crests and troughs of the attached internal waves. On the whole, according to linear theory, the calculations of the phase surfaces of the internal wave shapes [30,31,68] are consistent with the visualization images, even at the smallest values of the body velocity [69]. Here and below, the ligaments are presented by thin interfaces separating the internal waves and density wake.

The images of the electrolytic precipitation suspension, shown in Figure 8, illustrate the spatial geometry of the density wake past a slowly moving sphere (and small value of the Froude number, respectively). Fine particles are formed on the transverse tin belt.

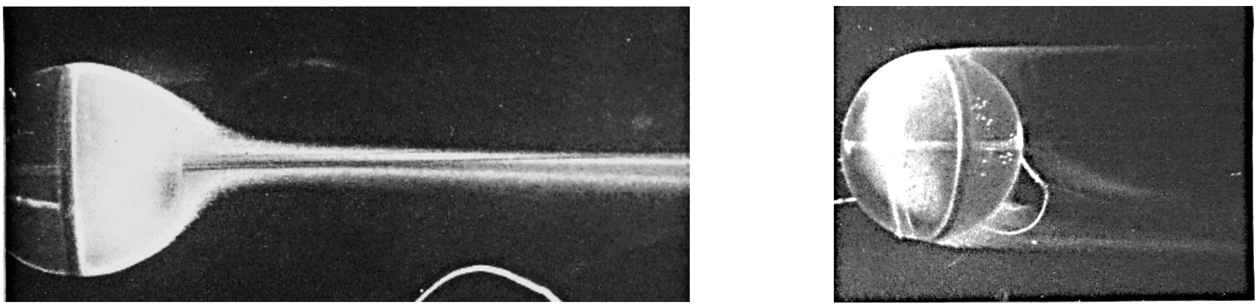

(**a**) (**b**)

Figure 8. Patterns of electrolytic precipitation suspension past a slowly moving sphere in CSF, $T_b = 4.5$ s, $N = 1.4$ s^{-1}, $D = 5$ cm, $U = 0.03$ cm/s, $\mathrm{Re} = UD/\nu = 15$, $\mathrm{Fr} = 1.8 \times 10^{-5}$; (**a**,**b**) top and side view.

In the top view, the dense suspension is distributed evenly over the surface of the sphere and the plane wake. In the side view, only the edges of the wake are colored. They are in contact with the sphere poles. The sharpness of the separation lines on the sphere surface indicates the planar geometry of the shells bounding the wake. They are formed by converging flows, which sharpen DiF on the impermeable sphere surface. The general shape and the narrowness of the colored wake in the horizontal plane as well as the high altitude in the vertical plane determine the selection of a rectangle for approximating the cross-sectional shape of the density wake [69,70]. The maximum suspension concentration is observed on the edges of the rectangular flow section.

The discrete symmetry of the cross-section shape of the wake with respect to the horizontal and vertical planes, which passes through the motion line of the body center, indicates the dominance of the buoyancy effects over inertial and nonlinear effects. Their symmetry reflects the perfect continuous symmetry of the body. The initial density gradient intensification in the vicinity of the body enhances the consequences of buoyancy effects in the creeping flow mode. At low velocities of the sphere, the liquid mainly flows around an obstacle along isopycnal (close to horizontal) lines.

Structural differences in the geometry of the flow components become more distinct with an increasing sphere velocity [70]. In the schlieren flow pattern in Figure 9a, the blocked fluid is visualized by dark and light spots in front of the body. They are bounded by tilted rays of non-stationary internal waves extending from the poles of the sphere.

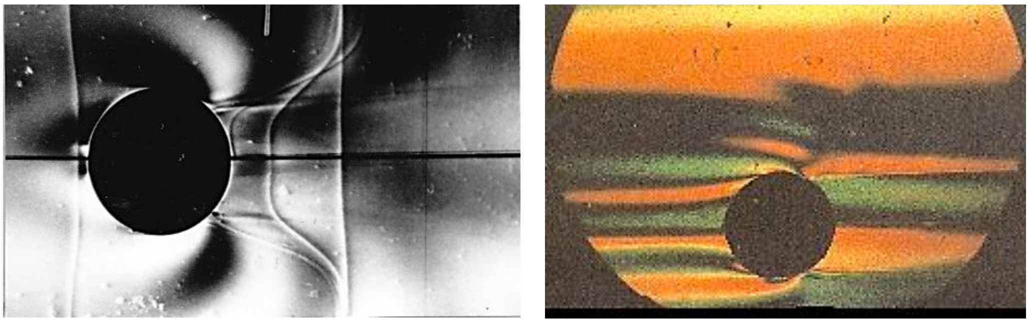

(**a**) (**b**)

Figure 9. Schlieren images of a stratified flow around a uniformly moving sphere at small Froude numbers: (**a**) $T_b = 12.0$ s, $N = 0.52$ s^{-1}, $D = 4$ cm, $U = 0.43$ cm/s, Re = 132, Fr = 0.04, (**b**)$T_b = 3.0$ s, $N = 2.09$ s^{-1}, $D = 5$ cm, $U = 0.5$ cm/s, Re = 250, Fr = 0.002.

Curvilinear bands extending from the separation points of sharp almost horizontal interfaces on the rear part of the sphere represent attached internal waves. The fine interfaces outline the density wake. The sharpness of the boundaries separating the domains with different kinds of a flow demonstrates strong interaction between the fine ligaments with more long internal waves [71] in different flow regimes past a sphere [69,72].

The three successive curved vertical lines in Figure 9a are deformed markers, which create the arising gas bubbles [59]. The vertical line is the initial bubble wake deformed by the shear flow with time. A profile with an almost uniform central part surrounded by two inclined sections visualizes the constant velocity in the center of the wake inside two wide shear layers. The third marker line directly adjacent to the surface of the body illustrates the patterns of velocity distribution on the boundaries of the wake. Here, the heights of the velocity shear layers and the thickness of the ligaments submerged in their central parts differ in more than an order of magnitude, as in the nonstationary DiF (Formulas (2) and (3)).

With a further increase in the velocity of the body, the length and amplitude of the attached waves grow. A group of five attached waves is presented in Figure 9b. The shapes of the color bands ahead and past a sphere reflect the difference in upstream and downstream density profiles. A more homogeneous domain of a blocking fluid is bounded by non-stationary waves. Behind the body, the ligaments forming the density wake envelopes are expressed. The linear theory for the uniform motion of the sphere satisfactorily describes the phase surfaces of the attached waves, both along a horizontal [31,68] and an inclined trajectory [32]. The selection of the position and the intensity of the model sources and sinks allows achieving satisfactory agreement between the numerical and measured displacement amplitudes [32,68].

With an increase in the body velocity at Fr << 1, the length and amplitude of all types of internal waves increase. It concerns non-stationary upstream waves, attached downstream, and trapped waves inside a density wake with their own profiles of velocity and density. The trapped waves inside the wake correspond to a set of tilted antisymmetric dark and light bands past the body, limited by high-gradient diverging interfaces in Figure 10a.

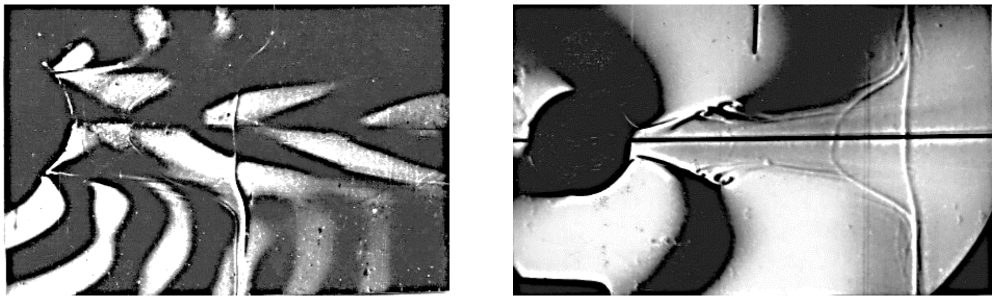

(**a**) (**b**)

Figure 10. Schlieren images of a stratified flow around a uniformly moving sphere: (**a**) $T_b = 3.0$ s, $N = 2.09\ \text{s}^{-1}$, $D = 5$ cm, $U = 0.76$ cm/s, Fr = 0.005, Re = 384; (**b**) $T_b = 12.0$ s, $N = 0.52\ \text{s}^{-1}$, $D = 4$ cm, $U = 0.8$ cm/s, Re = 256, Fr = 0.15.

The curvilinear phase surfaces of the attached waves adjoin the wake boundaries almost vertically. Their contour is distorted by the shear flow at the wake boundary, the height of which noticeably exceeds the thickness of the interfaces.

A further increase in the body velocity enhances the generation of waves, sharpens the gradients in the wake envelope, and activates the interaction between the various components of the flow. At first the wake expands uniformly with distance from the body and then contracts in accordance with the wave pattern (Figure 10b). The wake envelopes become wavy with sharpened crests and flattened troughs.

The deformation of the density marker indicates that the flow velocity profile in the wake changes from a stepped profile (in Figure 9a) to a profile of Poiseuille's type (in Figure 10b). At the same time, the retained sharpness of the envelopes maintains a generally rectangular cross-sectional shape of the density wake. The shear flow at the top of the wake expansion folds its high-gradient envelopes into pronounced flat vortices with a horizontal axis (Figure 10b).

Although the thickness of the ligaments, which confine the wave field, is much smaller than the length of waves, they limit the propagation of waves rather efficiently. The sharpness of the boundary indicates the effectiveness of the interaction of the different length-scale components of the flows. They are waves and ligaments consisting of a complete solution of the system of fundamental equations [8,27,71].

The spatial structure of the flow in this range of parameters is illustrated by patterns of electrolytic precipitation, shown in Figure 11. Plane convex separation lines on the surface of the sphere outline the flatness of the upper horizontal "lids" of the density wake. Two vertical convex separation lines, indicating the flatness of the lateral border of the density wake, are also distinct.

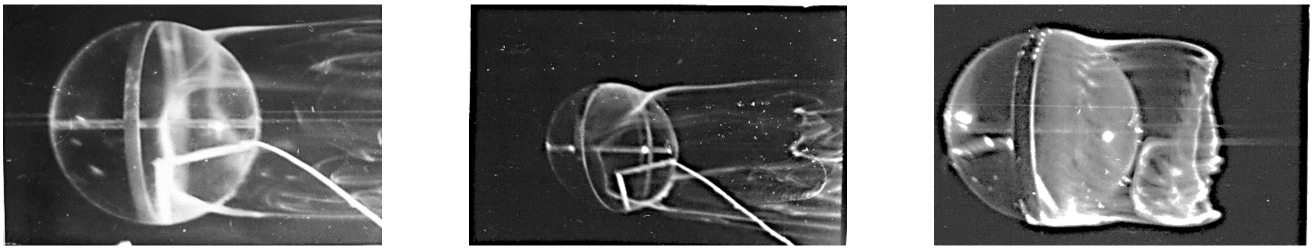

(**a**) (**b**) (**c**)

Figure 11. Electrolytic precipitation of a stratified flow past a uniformly moving sphere at small Froude numbers: (**a**)$T_b = 4.5$ s, $N = 1.4\ \mathrm{s}^{-1}, D = 5$ cm, $U = 0.7$ cm/s, Re = 350, Fr = 0.01; (**b**) $T_b = 5.0$ s, $N = 1.3\ \mathrm{s}^{-1}, D = 5$ cm, $U = 0.76$ cm/s, Re = 380, Fr = 0.013; (**c**) a homogeneous fluid, $N = 0, D = 5$ cm, $U = 0.70$ cm/s, Re = 350.

As the sphere velocity increases, the horizontal planes of the wake boundary approach each other, while the vertical ones diverge (Figure 10b). Here, the shape of the wake cross-section is close to a squared one. Four extended edges are formed by contacting flat upper horizontal and lateral envelopes of the wake. Their convex lines of intersection with the surface of the sphere and the straightness of the extended edges allow us to consider the shape of the density wake as a vertically compressed prism.

At the right boundary of the wake, the leading parts of the vertical "vortex columns", separated from the sidewalls of the density wake, are visible.

The electrolytic precipitation visualization of the spatial structure of the flow past a uniformly moving sphere in a homogeneous fluid at close values of the Reynolds number is shown for comparison in Figure 11c.

Here, the suspension carried by the flows from the transverse equatorial annular belt is uniformly distributed over the surface of the sphere and forms an annular separation line. In the vicinity of the separation line, the uniformity of the suspension is disturbed; it is redistributed in the form of more densely colored line segments and empty intervals between them. We have to study further whether the flow pattern indicates the formation of a "grooved" shape of the separation line of the cylindrical density wake, or whether such an impression is created by the play of light and shadows on the unevenly distributed density of the suspension, and thus the cylindrical shell itself is smooth. The circular contraction of the right edge of the suspension in the wake specifies the action of an axisymmetric toroidal vortex behind the sphere, which was repeatedly observed in the visualization of flows in experiments [12] and numerical simulations [44].

The prismatic wake in this flow regime is filled with pairs of "vertical vortex columns" (Figure 12a). Vortices are cut from below and above by the ligaments, which are the horizontal interfaces shown in the schlieren images (Figure 10). The flow in the wake has a complex three-dimensional character: individual, brightly colored fibers and surfaces with a complex shape and variable curvature, twisting into spirals, are distinguished in a distribution pattern in the visualized suspension. The vortex columns with flattened inner walls are separated by a faster narrow jet in the central part of the wake (see Figure 12b).

Successive frames of the flow pattern show that the entire vortex structure is stretched in a longitudinal direction and slowly oscillates in a transverse direction (Figure 13). We observe the proper structuralization of the suspension, which is initially uniformly distributed along the surface of the sphere. Here, dense threads are pronounced on weakly colored curvilinear surfaces.

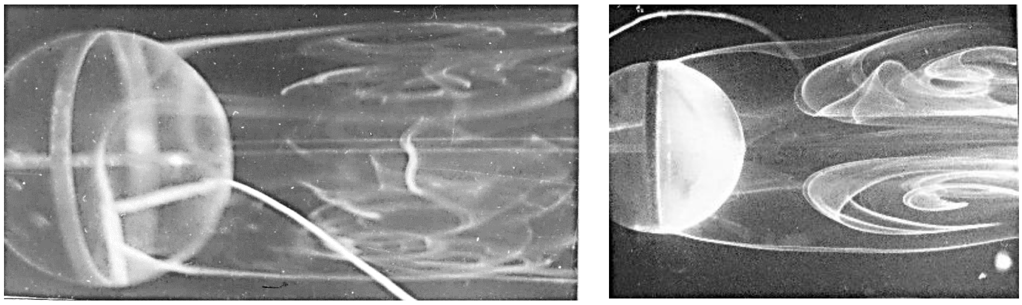

(**a**) (**b**)

Figure 12. Pattern of electrolytic precipitation suspension in "vertical vortex columns" in the wake past a sphere $(T_b = 4.5\text{ s};\ N = 1.4\text{ s}^{-1};\ D = 5\text{ cm})$: (**a**) side view $U = 0.7\text{ cm/s},\ \text{Re} = 350; \text{Fr} = 0.01$; (**b**) top view $U = 0.62\text{ cm/s}; \text{Re} = 310; \text{Fr} = 0.008$.

Figure 13. Evolution of an electrolytic precipitation suspension pattern in the wake past a sphere in CSF (top view): $T_b = 8.0$ s, $N = 0.785\text{ s}^{-1}$, $D = 5$ cm, $U = 0.65\text{ cm/s},\ \text{Re} = 325; \text{Fr} = 0.027$; time interval between frames $\Delta t = 1$ s.

The flow pattern loses regularity with a further increase in the flow velocity. The vertical separation line of the suspension from the surface of the sphere begins to elongate and approaches the separation point of the edges from above, forming the characteristic intersection of the dyed lines (Figure 14).

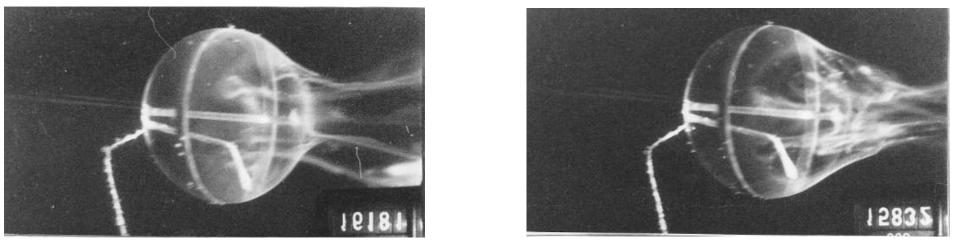

(**a**) (**b**)

Figure 14. The shape of the separation lines of the suspension from the sphere and the edges of the wake in the "expanding rectangle" stage in transient regime: (**a**,**b**) $T_b = 4.5;\ 9.0$ s, $N = 1.4;\ 0.7\text{ s}^{-1}$, $D = 5$ cm, U =1.08; 1.96 cm/s, Re = 540; 980 Fr = 0.02; 0.32.

The structure of the vortices in the wake is reconstructed with an increase in the sphere velocity and a decrease in the flow separation region height. In this case, a thin layer at the upper and lower envelopes of the wake expansion areas is firstly twisted into a spiral, the position of which is synchronized with the phase of the attached internal wave (crest in the upper hemi-space and trough in the lower one in Figures 10b and 15a).

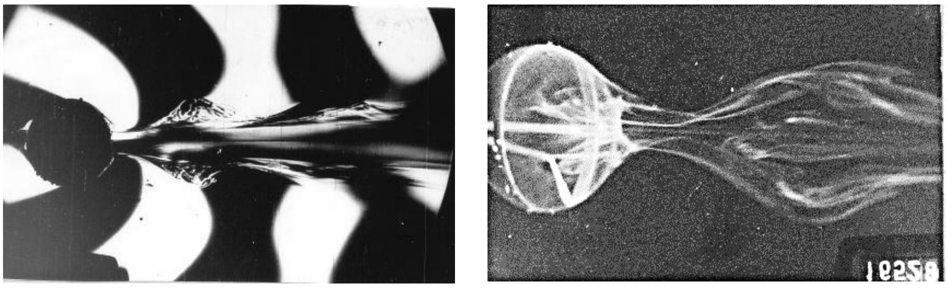

(**a**) (**b**)

Figure 15. Formation of a "vortex bubble" frozen in the field of attached internal waves by a pair of vortices with a horizontal axis: (**a**) conventional schlieren image with Foucault knife: $T_b = 3.0$ s; $N = 2.09$ s^{-1}; $D = 4$ cm; $U = 1.37$ cm/s, $\mathrm{Re} = 750$, $\mathrm{Fr} = U^2/N^2D^2 = 0.03$; (**b**) electrolytic precipitation $T_b = 9$ s, $N = 0.7$ s^{-1}; $D = 5$ cm; $U = 1.38$ cm/s, $\mathrm{Re} = 690$, $\mathrm{Fr} = 0.15$.

As the sphere velocity and Froude number increase, the vortex with a horizontal axis thickens and captures an increasing part of the "vortex bubble" (Figure 15a). Pronounced edges and individual lines emphasize the flatness of the wake boundaries. With distance, the flow degenerates with the formation of elongated horizontal interfaces and fibers throughout the volume of the wake. The inner structure and outer contour of the wake are visualized by the suspension of electrical precipitation in Figure 15b.

The black-and-white replica of the color schlieren image (Figure 16) shows that after the collapse of the "vortex bubble", the surface of the wake remains wavy [72]. The flow degenerates with the formation of elongated horizontal interfaces and filaments throughout the volume of the wake.

Figure 16. Black and white replica of the color schlieren image of the flow in the wake of the sphere: $T_b = 3.0$ s, $N = 2.09$ s^{-1}, $D = 4$ cm, $U = 1.45$ cm/s, $\mathrm{Re} = 780$, $\mathrm{Fr} = 0.03$.

The shapes of waves and vortices in the colored schlieren images differ significantly from the traditional schlieren patterns with the Foucault knife (Figure 15). It allows estimating the position of the high-gradient interfaces and the general deformation of the density profile.

8. Cylindrical Shape of the Wake Past a Sphere at High Froude Number

A further increase in the flow velocity is accompanied by a qualitative change in the flow structure. The inertial and nonlinear effects gradually become more pronounced and dominate over the effects of stratification, and they even enhance with the formation of high-gradient interfaces. The large length of the internal wave, which exceeds the diameter of the sphere in Figure 17 at almost an order of magnitude, indicates a violation of the spatial synchronism condition, which is necessary for the effective generation of waves. The attached wave amplitude decreases rapidly with a further-increasing Froude number. The weakening of the attached wave does not ensure the fulfillment of the condition of their spatial synchronization with the wake boundary geometry, which is defined by the positons of the vortices.

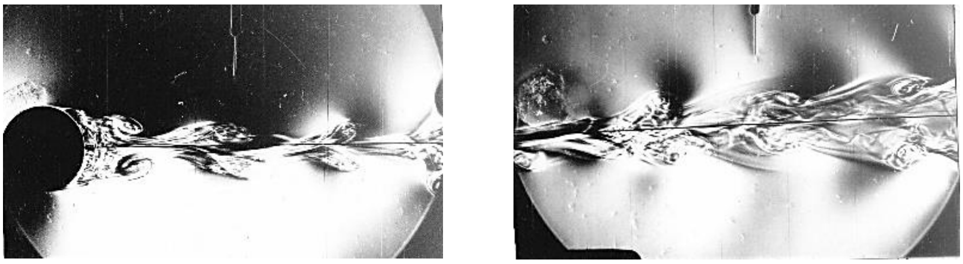

(**a**) (**b**)

Figure 17. Schlieren images of periodically separating axisymmetric vortices from the flow at the rear part of the sphere in a weakly CSF: $T_b = 12$ s, $N = 0.52$ s^{-1}, $D = 4$ cm, $U = 2.1$ cm/s, Re = 840, Fr = 1.02; (**a**,**b**) $t = 0$; 4.5 s.

The length of the region of increased vorticity in the rear part of the sphere increases. Having reached a critical size, the bottom vortex splits up and its outer part is thrown into the wake in the form of a toroidal ring with a conical front part (Figure 17). Here, the position of the inner vortex structures is determined predominantly by dynamic conditions. Moving separated vortices covered by sharp envelopes emit internal waves similar to the waves of a solid body. Bands, visualized in black-and-white images, of the internal waves around the wake are tilted in the direction of the body motion (the geometry and dynamics of a free laminar vortex ring motion in a CSF were studied in detail in [73]).

As the density gradient increases, so does the frequency of vortex shedding, the intensity of short internal waves generated by the separate vortices, and the degree of manifestation of fine structures. The resulting ligaments, which correspond to the fibers and interfaces in the schlieren image (Figure 18), extend in the direction of body motion.

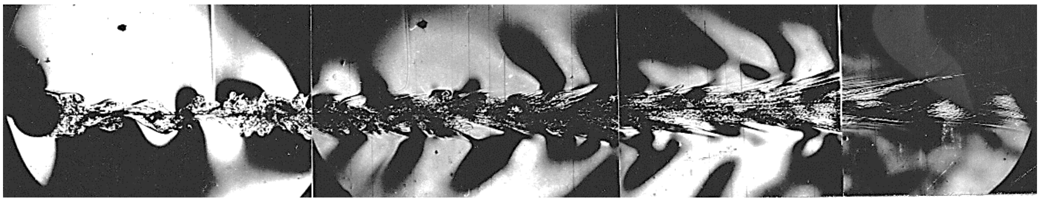

Figure 18. Coalescence of separated vortices into density wake with irregular envelope: $T_b = 3.5$ s, $N = 1.8$ s^{-1}, $D = 3$ cm, $U = 6.8$ cm/s, Re = 2040, Fr = 1.6.

The difference between the attached internal waves generated by the body itself [68], with the length proportional to its velocity $\lambda = UT_b$, and the short non-stationary waves emitted by vortices in the wake, are clearly expressed in the flow pattern in Figures 17 and 18.

With a further increase in velocity, the structure of the wake boundary changes and the vortices are merged into a single wake with a continuous envelope (Figure 19). However, the existence and the periodicity of the location of radiating vortices in the wake indicate the regularity of the pattern of short internal waves.

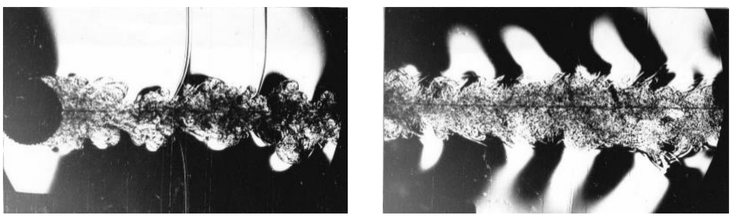

Figure 19. Irregular axisymmetric vortex wake past a sphere: $T_b = 3$ s, $N = 2.09$ s^{-1}, $D = 4$ cm, $U = 8.7$ cm/s, Re = 3488, Fr = 1.1, $\Delta t = 1.5$ s.

An oscillating wake is observed behind a uniformly moving sphere along with an axisymmetric pulsating wake. In this regime, vortices periodically separate from a flow directly past a sphere and propagate along a sloping trajectory at the separation region (Figure 19). Perfect axial symmetry of the wake is lost. When the excess lateral momentum is carried away by the radiated internal waves, the detached vortex rings return to the center of the flow. In this case, as well as in previously considered flow patterns, the ligaments, which are high-gradient envelopes, form a boundary separating the vortices from the radiated waves. Here, the mechanical action of the ligaments is equivalent to the surface of a solid body impact.

Consideration of the data presented in Figures 7–20 shows that two types of symmetries are distinguished in the wake flow past a uniformly moving sphere. A rectangular wake with a discrete symmetry is observed at small Froude numbers (Fr $<<$ 1). A round wake is formed at large Froude numbers (Fr $>$ 1).

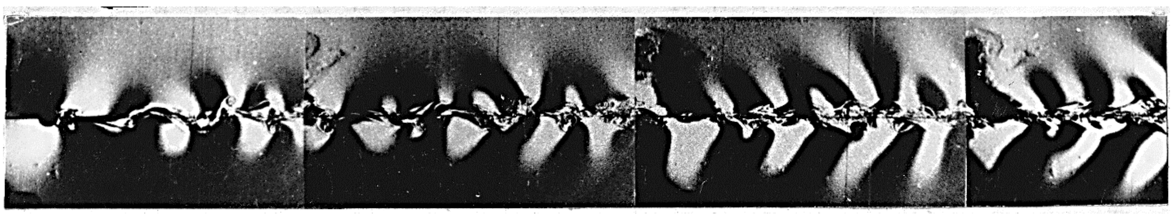

Figure 20. Oscillating vortex wake behind a sphere of a small diameter in CSF: $T_b = 3.5$ s, $N = 1.8\ \mathrm{s}^{-1}$, $D = 1$ cm, $U = 7.4$ cm/s, Re = 742, Fr = 17.

The scheme of the flow past a sphere at intermediate Froude and Reynolds numbers is close to a rectangular form. A transverse cross-sectional view of the density wake is shown in Figure 21. The position of the long side depends on the value of the Froude number (or velocity for a constant body diameter).

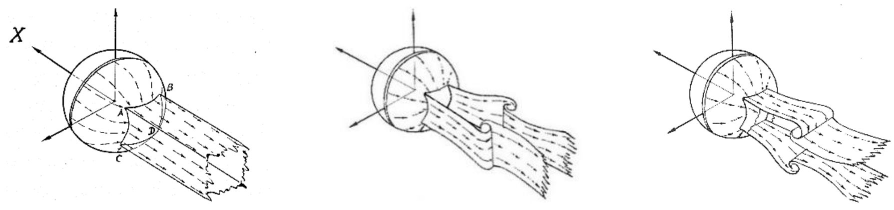

(**a**) (**b**) (**c**)

Figure 21. Scheme of the vortex flow past a sphere, (**a**) rectangular density wake, (**b**) wake with submerged vertical vortex columns, (**c**) wake with horizontal rotors.

At the smallest values of the sphere velocity, when buoyancy effects dominate, the rectangle is elongated vertically. If the generation of vorticity in a shear flow at the vertical boundaries of the wake is supplemented by the action of the baroclinic mechanism due to the multidirectional pressure and density gradient vectors [13], it leads to the formation of vortex pairs.

In this flow, the particles move mainly along isopycnal trajectories. The axes of the downstream symmetric "vortex columns" are oriented vertically.

Flat inner boundaries of the vortices in Figures 12b and 13 visualize the central back jet in the wake. With increasing velocity, inertial effects pull the upper and lower separation lines to the center and push the side faces apart (a wake scheme with a square section is shown in Figure 2a). Gradually, slides of the vertical envelopes are separated and twisted in vertical vortex columns, as shown in Figure 2b.

Increased stratification on the horizontal wake "lids" hinders the formation of large eddies with a horizontal axis that moves fluid to the horizons of neutral buoyancy. Deviations in the position of the boundary from the horizontal axis practically stop the removal of the vorticity from the wake. The vorticity turns out to be “frozen” in the wake, as in case of the particles of the suspension being transferred.

A gradual increase in velocity and Froude number leads to further contraction of the separation region height and “twisting” into a thin vortex curl of high-gradient interfaces at the horizontal boundaries of the wake. Vorticity in horizontal rotors is higher than in the “vertical vortex columns”. Large vertical vortices are destroyed and replaced by intensive horizontal rotors (Figure 21c). A more intense vortex motion leads to the destruction of corners and edges of the wake and the formation of a toroidal bottom vortex behind the sphere, as in a homogeneous liquid.

The dependence of the angular position of the horizontal separation lines on the surface of a sphere with a diameter of 4 cm in a weakly CSF with a buoyancy period of = 12 s on the Froude number is shown in Figure 22 (the angle is measured from the horizontal position). Measurements of the separation angles of the wake envelopes in the central vertical plane were made according to three types of schlieren visualization: traditional (vertical slot—Foucault knife), slot-thread set at an angle of 45°, and color schlieren method. On the decreasing and increasing parts of the curve, the data of the independent measurements agree with each other.

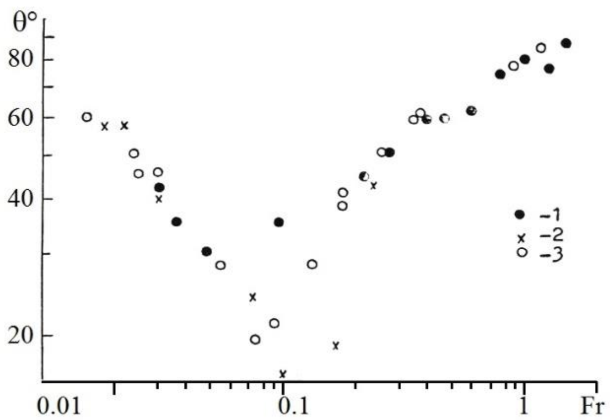

Figure 22. Separation angle of the density wake envelope on a sphere in a weakly CSF versus Froude number ($T_b = 12$ s $D = 4$ cm): visualization: 1—slit-Foucault knife; 2—slit-thread; 3—“natural rainbow” color schlieren method.

Particularly, the separation angle variations in the density wake on spheres of different diameters in the side schlieren view are shown in Figures 23 and 24. At the lowest values of the Froude number, the separation angle of the wake envelope from the sphere in the vertical plane is close to the normal quantity, θ ∼90°, and in the horizontal plane it does not exceed $\varphi < 15°$, which corresponds to the vertical rectangle for the cross-section of the wake. As the body velocity increases, the separation angle in the vertical plane decreases, and in the horizontal plane it increases, and exceeds the vertical one, θ ∼45°, and $\varphi = 67°$ at Fr = 0.03. The shape of the wake cross-section is a rectangle, elongated horizontally.

The experimental data in these figures are approximated by power-law functions of the form $\theta = A_R(\mathrm{Re})^r$ and $\theta = A_F(\mathrm{Fr})^m$. Exponents and coefficients in these formulas depend on other parameters of the problem.

In the interval of the Froude number, when the height of the separation region decreases with the velocity increases, their values are distinguished and equal: $r = -1.25$, $m = -0.66$ ($T_b = 12$c, $D = 4$ cm); $r = -1.7$, $m = -077$ ($T_b = 3$ c, $D = 2$ cm); $r = -0.48$, m = −0.35 ($T_b = 3$ c, $D = 4$ cm).

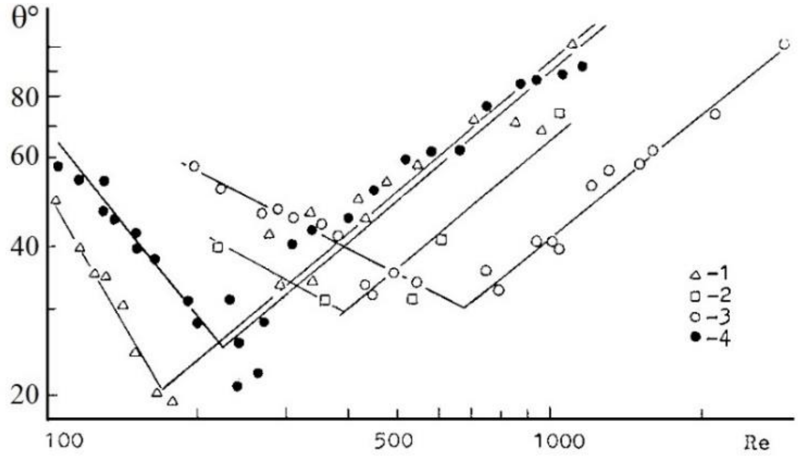

Figure 23. Separation angle of the density wake envelope on a sphere versus Reynolds number: curves (1–3)—$T_b = 3$ s, $D = 2, 3, 4$ cm; (4)—$T_b = 12$ s, $D = 4$ cm.

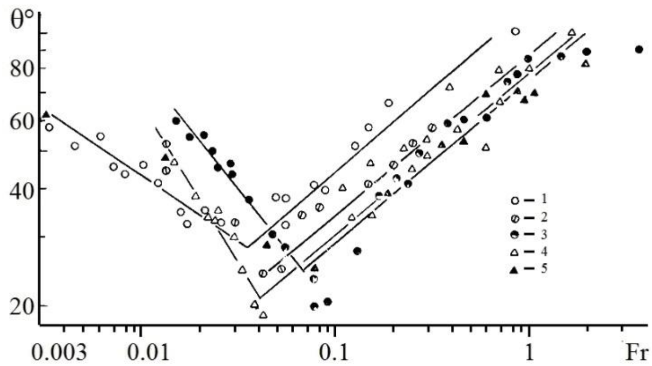

Figure 24. Separation angle of the density wake envelope on a sphere versus Froude number: curves 1 $T_b = 3.5$ s, $D = 4$ cm; 2—$T_b = 4.5$ s, $D = 4$ cm; 3—$T_b = 12.0$ s, $D = 4$ cm; 4—$T_b = 3.0$ s, $D = 2$ cm; 5—$T_b = 4.1$ s, $D = 2$ cm.

If the Froude number exceeds the critical value of the minimum wake height, the exponents is $m = 0.5$ in the approximation of the separation angle on the Reynolds and Froude numbers in all experiments performed at various values of the buoyancy period and sphere diameter.

At the lowest values of the Froude number, the separation angle of the wake envelope from the sphere in the vertical plane is close to normal, $\theta \sim 90°$, and in the horizontal plane, it does not exceed $\varphi < 15°$, which corresponds to the vertical rectangle for the cross-section of the wake. As the body velocity increases, the separation angle in the vertical plane decreases; in the horizontal plane it increases, and exceeds the value in vertical plane $\theta \sim 45°$ and $\varphi = 67°$ at $\mathrm{Fr} = 0.03$. The shape of the wake cross-section is a rectangle, which is elongated horizontally.

The given values of the separation angle of the wake from a sphere for different values of the Froude and Reynolds numbers are consistent with the results [40] obtained for a sphere with a diameter $D = 6.36$ cm/s.

The clarity of the shape is ensured by an increased concentration of the suspension on the edges of the wake and the small thickness of its boundaries (horizontally and vertically oriented high-gradient interfaces). The dependences of the boundary parameters and fine geometry of the flow on the properties of the medium and the conditions of motion of the body require a more detailed study.

At high body velocities, when the Froude number becomes greater than one, a cylindrical wake, filled with small-scale disturbances, is formed. The wake is separated from the annular toroidal vortex in the rear part of the sphere (Figure 19).

Having reached critical values, the vortex, contoured by high-gradient envelopes, breaks off and drifts in the wake. It remains connected to the flow past a sphere by a conical set of ligaments. Moving vortices radiate transient internal waves. Their rays, which represent phase surfaces, are oriented to the body motion. The vortices are gradually slowed down, deformed, and pulled out by the unsteady flow in the wake. The spiral interfaces of the vortex are elongated; they form line structures that connect the remains of the vortex rings into a single system.

9. Results and Discussion

The results of the first regular studies of the stratified fluid flows around 2D and 3D obstacles focused on visualizing the spatial structure of dispersive internal waves. They have been summarized in monographs [30,74], which maintained their cognitive value. An extensive series of experimental studies of the flow around a sphere uniformly moving in a pool filled with a stratified fluid were independently carried out in several countries: the USSR [34,68–72], the USA [75–78], France [79–82], and Great Britain [33,38]. In the experiments, flow patterns were visualized using high-resolution classical [3,4] and modified schlieren methods [25], including the density gradient registration instruments, modified for background continuous density distribution [34]; direct shadowgraph observations [75]; dyeing by common and fluorescent impurities; particle tracing (particle streak photograph) [76–78]; and electrolytic precipitation [69,70].

The experiments have shown that at low values of the Froude number, when the buoyancy effects dominate, the density wake has a prismatic shape. It is elongated vertically at first, then its cross-section becomes square [69], and, finally, it becomes flattened under the action of inertial effects at a range of Froude numbers, $0.03 < \mathrm{Fr} < 0.09$. The observed discrete symmetry of the wake is consistently reproduced in independent experiments.

The flat boundaries of such a density wake are formed by ligaments, i.e., high-gradient interfaces that arise in the flow in the vicinity of the sphere surface. The interfaces are located inside a thicker shear layer of velocity. The height of the shear layer in a liquid with a large Schmidt number ($\mathrm{Sc} = 700$ for an aqueous solution of sodium chloride, which is used in most experiments) is at least an order of magnitude greater than the ligaments thickness. Similar ratios of heights were observed in an unsteady DiF on the impermeable obstacle. The effects of amplification of the gradients at the wake boundaries have been registered in [34].

Classical schlieren methods have the highest sensitivity and spatial resolution among those listed above. These methods enable us to record disturbance patterns in the entire range of flow parameters (from the slowest ones induced by diffusion on topography to fast vortex flows) and to resolve all structural components in the studied flows. The low sensitivity of the direct shadow and moiré methods does not let us visualize weak internal waves and fine high-gradient interfaces, which was noted in [75]. The discrete nature of a number of flow visualization methods, in particular, using tracing particles for velocity measurement and the flow visualization (particle streak photograph) [78–80], does not allow us to register thin interfaces and assess their effect on the flow structure.

As the Froude number increases, the sidewalls of a rectangular wake begin to split, and form two and more vertical vortex columns [72] (lee-side eddies in the terminology of [75]) in the downstream wake.

The joint action of the velocity shear and pressure perturbations in the field of intense attached internal waves leads to the formation of “vortex bubbles” with a horizontal axis of symmetry. The sets of complete solutions of the system of fundamental Equation (1) contain functions that describe both periodic components—waves and vortices—as well as a large number of ligaments that characterize the thin high-gradient interfaces and fibers [8,27].

As vorticity accumulates in the rear part of the flow past the body, the wake faces become rounded and take a cylindrical shape. All the structural components, including ligaments, take part in nonlinear interactions with each other, with waves and mean flow. It provides a variety of available scenarios for the evolution of stratified flows.

The classification of the sequence of the vortex structures in the transitional flow regime was first presented in [75]. The pattern of the vortex structure near and far from the obstacle has been described in great detail in subsequent experiments [81,82]. The evolution of the fine structure of the density profiles downstream in the wake, revealed by a high-resolution electrical conductivity sensor, enabled studies of the dynamics of submerged vortices [83]. In a number of experiments, the pattern of internal waves [84] and the global structure of the vortex and turbulent wake were elucidated [85,86].

Analytical [87], numerical [88–91], and experimental studies [41,42] of the internal wave field and the generally round turbulent wake behind a rapidly moving sphere in a CSF are being actively pursued using various approaches.

10. Conclusions

Fluid stratification, even if it is weak, significantly affects the structure, symmetry, and dynamics of the flow past a uniformly towed sphere. At low values of the Froude number, ligaments that are high-gradient interfaces enhance the effect of stratification. Horizontal and vertical envelopes bound a narrow prismatic density wake past a slowly moving body.

With an increase in sphere velocity, the shape of the transverse cross-section of the wake transforms from a vertically elongated rectangle into a square and then into a narrow horizontally elongated rectangle. In a high wake, paired vertical vortex columns are formed. They are enclosed between the horizontal interfaces and form envelopes of the density wake.

Vortices with a horizontal axis, which are immersed in a horizontally stretched wake, lead to a periodic increase in its vertical size. The position of the wake expansion and compression regions is consistent with the phase pattern of the attached internal waves.

At large values of the Froude number, the accumulation of vorticity, accompanied by the formation of a toroidal vortex in the rear part of the sphere, causes a rearrangement of the discrete symmetry of the density wake into a continuous axisymmetric one. In the phase of flow restructuring, various forms of vortex components, contoured by thin high-gradient envelopes, are observed in the wake.

Funding: This research received no external funding.

Institutional Review Board Statement: Not applicable.

Informed Consent Statement: Not applicable.

Acknowledgments: The work was carried out as a state assignment (state registration No. AAAA-A20-120011690131-7). I thank E.Y. Sysoeva for assistance in conducting experiments.

Conflicts of Interest: The author declares no conflict of interest. The funders had no role in the design of the study; in the collection, analyses, or interpretation of data; in the writing of the manuscript, or in the decision to publish the results.

References

1. Popov, N.I.; Fedorov, K.N.; Orlov, V.M. *Sea Water*; Nauka: Moscow, Russia, 1979; 330p. (In Russian)
2. Franklin, B. Behavior of oil on water. Letter to J. Pringle. In *Experiments and Observations on Electricity*; R. Cole: London, UK, 1769; pp. 142–144.
3. Vasiliev, L.A. *Shadow Methods*; Nauka: Moscow, Russia, 1968; 400p. (In Russian)
4. Settles, G.S. *Schlieren and Shadowgraph Techniques: Visualizing Phenomena in Transparent Media*; Springer Science & Business Media: Berlin, Germany, 2001; 376p.
5. Chashechkin, Y.D.; Prokhorov, V.E. Visualization and echo sounding of stratified fluid disturbances in front of and behind a vertical plate. *Dokl. Phys.* **2020**, *65*, 178–182. [CrossRef]
6. Pao, H.-P.; Lai, R.Y.; Schemm, C.E. Vortex trails in stratified fluids. *J. Hopkins APL Techn. Digest* **1982**, *3*, 12–18.
7. Strutt, J.W.; Rayleigh, L. Investigation of the character of the equilibrium of an incompressible heavy fluid of variable density. *Proc. Lond. Math. Soc.* **1883**, *4*, 170–177.
8. Chashechkin, Y.D. Foundations of engineering mathematics applied for fluid flows. *Axioms* **2021**, *10*, 286. [CrossRef]
9. Prandtl, L. *The Essentials of Fluid Dynamics*; Blackie & Son Ltd.: London, UK, 1953; 452p.
10. Landau, L.D.; Lifshitz, E.M. *Fluid Mechanics. V.6. Course of Theoretical Physics*; Pergamon Press: Oxford, UK, 1987; 560p.

11. Mossa, M. The recent 500th anniversary of Leonardo da Vinci's death: A reminder of his contribution in the field of fluid mechanics. *Environ. Fluid Mech.* **2021**, *21*, 1–10. [CrossRef]
12. Van Dyke, M. *An Album of Fluid Motion*; Parabolic Press, Inc.: Stanford, CA, USA, 1982; 176p.
13. Kochin, N.E.; Kibel, I.A.; Rose, N.V. *Theoretical Hydromechanics. Part 1*; OGIZ. Gostekhizdat: Leningrad-Moscow, USSR, 1948; 728p. (In Russian)
14. Birkhoff, G. *Hydrodynamics. A Study in Logic, Fact and Similitude*, 2nd ed.; Princeton University Press: Princeton, NJ, USA, 1960; 184p.
15. Bernoulli, D. *Hydrodynamica, Sive de Viribus et Motibus Fluidorum Commentarii, Opus Academicum*; Sumptibus, J.R., Ed.; Argentorati: Dulseckeri, The Netherlands, 1738; 304p.
16. Robins, B. *New Principles of Gunnery*; J. Nourse: London, UK, 1742; 160p.
17. Euler, L. *Neue Grundsätze der Artillerie. Aus dem Englischen des Herrn Benjamin Robins Übersetzt und mit Vielen Anmerkungen Versehen*; Haude Königl. und der Academie der Wissenschaften: Berlin, Germany, 1753; 480p.
18. D'Alembert, J.-L.R.; la Marquis de Condorcet, J.M.A.; l'abbe Bossut, C. *Nouvelles Expériences sur la Résistance des Fluids*; C.-A. Jombert: Paris, France, 1777; 232p.
19. D'Alembert, J.-L.R. *Réflexions sur la Cause Générale des Vents*; David: Paris, France, 1747; 372p.
20. Euler, L. Principes généraux du mouvement des fluids. *Mémoires L'académie Des. Sci. Berl.* **1757**, *11*, 274–315.
21. Fourier, J.B.J. *Théorie Analytique de la Chaleur*; Firmin Didot Père et Fils: Paris, France, 1822; 639p.
22. Navier, C.-L.-M.-H. Mémoire sur les Lois du Mouvement des Fluids. *Mém. l'Acad. Sci.* **1822**, *6*, 389–417.
23. Stokes, G.G. On the theories of the internal friction of fluids in motion, and of the equilibrium and motion of elastic bodies. *Trans. Camb. Philos. Soc.* **1845**, *8*, 287–305.
24. Stokes, G.G. On the Effect of the Internal Friction of Fluids on the Motion of Pendulums. *Trans. Camb. Philos. Soc.* **1850**, *9*, 1–141.
25. Chashechkin, Y.D. Schlieren visualization of stratified flow around a cylinder. *J. Visualiz.* **1999**, *1*, 345–354. [CrossRef]
26. Müller, P. *The Equations of Oceanic Motions*; CUP: Cambridge, UK, 2006; 302p.
27. Chashechkin, Y.D.; Zagumennyi, I.V. 2D hydrodynamics of a plate: From creeping flow to transient vortex regimes. *Fluids* **2021**, *6*, 310. [CrossRef]
28. Monin, A.C.; Yaglom, A.M. *Statistical Fluid Mechanics–Vol. 1: Mechanics of Turbulence*, 1st ed.; The MIT Press: Boston, MA, USA, 1971; 782p.
29. Chashechkin, Y.D.; Kistovich, A.V. Classification of three-dimensional periodic fluid flows. *Dokl. Phys.* **2004**, *49*, 183–186. [CrossRef]
30. Lighthill, J. *Waves in Fluids*; CUP: Cambridge, UK, 2001; 524p.
31. Makarov, S.A.; Chashechkin, Y.D. Apparent internal waves in a fluid with exponential density distribution. *J. Appl. Mech. Tech. Phys.* **1981**, *22*, 772–779. [CrossRef]
32. Smirnov, S.A.; Chashechkin, Y.D. Internal lee(joined) waves at an arbitrary orientation of the incident flow. *Izv. Atmos. Ocean. Phys.* **1998**, *43*, 475–482.
33. Scase, M.; Dalziel, S. Internal wave fields generated by a translating body in a stratified fluid: An experimental comparison. *J. Fluid Mech.* **2006**, *564*, 305–331. [CrossRef]
34. Chashechkin, Y.D.; Gumennik, E.V.; Sysoeva, E.Y. Transformation of a density field by a three-dimensional body moving in a continuously stratified fluid. *J. Appl. Mech. Tech. Phys.* **1995**, *36*, 19–29. [CrossRef]
35. Phillips, O.M. On flows induced by diffusion in a stably stratified fluid. *Deep-Sea Res.* **1970**, *17*, 435–443. [CrossRef]
36. Chashechkin, Y.D. Hydrodynamics of a sphere in a stratified fluid. *Fluid Dyn.* **1989**, *24*, 1–7. [CrossRef]
37. Greenslade, M. Drag on a sphere moving horizontally in a stratified fluid. *J. Fluid Mech.* **2000**, *418*, 339–350. [CrossRef]
38. Scase, M.; Dalziel, S. Internal wave fields and drag generated by a translating body in a stratified fluid. *J Fluid Mech.* **2004**, *498*, 289–313. [CrossRef]
39. Mason, P.J. Forces on spheres moving horizontally in a rotating stratified fluid. *Geoph. Astrophys. Fluid Dyn.* **1977**, *8*, 137–154. [CrossRef]
40. Lofquist, K.; Purtell, L. Drag on a sphere moving horizontally through a stratified liquid. *J. Fluid Mech.* **1984**, *148*, 271–284. [CrossRef]
41. Cocetta, F.; Gillard, M.; Szmelter, J.; Smolarkiewicz, P.K. Stratified flow past a sphere at moderate Reynolds numbers. *Comp. Fluids* **2021**, *226*, 104998. [CrossRef]
42. Madison, T.; Xiang, X.; Spedding, G. Laboratory and numerical experiments on the near wake of a sphere in a stably stratified ambient. *J. Fluid Mech.* **2022**, *933*, A12. [CrossRef]
43. Shirayama, S.; Kuwahara, K. Patterns of Three-Dimensional Boundary Layer Separation. In Proceedings of the AIAA 25th Aerospace Sciences Meeting, Reno, NV, USA, 12–15 January 1987. Preprint AIAA-87-0461, 10p.
44. Gushchin, V.A.; Matyushin, P.V. Numerical simulation of separated flow past a sphere. *Comp. Math. Math. Phys.* **1997**, *37*, 1086–1100.
45. Li, J.; Zhou, B. The symmetry and stability of the flow separation around a sphere at low and moderate reynolds numbers. *Symmetry* **2021**, *13*, 2286. [CrossRef]
46. Nakamura, I. Steady wake behind a sphere. *Phys. Fluids* **1976**, *19*, 5–8. [CrossRef]

47. Karyagin, V.P.; Lopatkin, A.I.; Shvets, A.I.; Shilin, N.M. Experimental investigation of the separation of flow around a sphere. *Fluid Dyn.* **1991**, *26*, 126–129. [CrossRef]
48. Gerasimov, S.I.; Faikov, Y.I. *Shadow Photography in a Divergent Beam of Light*; FSUE RFSC-VNIIEF: Sarov, Russia, 2010; 344p. (In Russian)
49. Fortuin, J. Theory and application of two supplementary methods of constructing density gradient columns. *J. Polym. Sci.* **1960**, *44*, 505–515. [CrossRef]
50. Oster, G. Density gradients. *Sci. Am.* **1965**, *217*, 70–75. [CrossRef]
51. Mowbray, D. The use of schlieren and shadowgraph techniques in the study of flow patterns in density stratified liquids. *J. Fluid Mech.* **1967**, *27*, 595–608. [CrossRef]
52. Chashechkin, Y.D. Colour Schlieren method. In *Optical Methods in Dynamics of Fluids and Solids*; IUTAM Symposium; Springer-Verlag: Berlin, Germany, 1985; pp. 275–282.
53. Sakai, S. Visualization of internal gravity waves by Moire-method. *Kashika-Joho* **1990**, *10*, 65–68.
54. Dalziel, S.B.; Hughes, G.O.; Sutherland, B.R. Whole-field density measurements by "synthetic schlieren". *Exp. Fluid.* **2000**, *28*, 322–335. [CrossRef]
55. Honji, H. Near wakes of a sphere in a stratified flows. *Fluid Dyn. Res.* **1987**, *2*, 75–76. [CrossRef]
56. Honji, H. Vortex Motions in the Stratified Wake Flows. *Fluid Dyn. Res.* **1988**, *3*, 425–430. [CrossRef]
57. Hydrophysical Complex for Modeling Hydrodynamic Processes in the Environment and Their Impact on Underwater Technical Objects, as Well as the Distribution of Impurities in the Ocean and Atmosphere, Institute for Problems in Mechanics RAS. Available online: http://ipmnet.ru/uniqequip/gfk (accessed on 15 June 2022).
58. Smirnov, S.A.; Chashechkin, Y.D.; Il'inykh, Y.S. High-accuracy method for measuring profiles of buoyancy periods. *Meas. Techn.* **1998**, *41*, 514–519. [CrossRef]
59. Il'inykh, A.Y.; Il'inykh, Y.S.; Chashechkin, Y.D. Measuring transducers of electrical conductivity of liquids. *Meas. Techn.* **2016**, *58*, 1336–1340. [CrossRef]
60. Linden, P.F.; Weber, J.E. The formation of layers in a double-diffusive system with a sloping boundary. *J. Fluid Mech.* **1977**, *81*, 757–773. [CrossRef]
61. Kistovich, A.V.; Chashechkin, Y.D. The structure of transient boundary flow along an inclined plane in a continuously stratified medium. *J. Appl. Maths. Mech.* **1993**, *57*, 633–639. [CrossRef]
62. Zagumennyi, I.V.; Chashechkin, Y.D. Diffusion induced flow on a strip: Theoretical, numerical and laboratory modeling. *Procedia IUTAM* **2013**, *8*, 256–266. [CrossRef]
63. Baidulov, V.G.; Matyushin, P.V.; Chashechkin, Y.D. Evolution of the diffusion-induced flow over a sphere submerged in a continuously stratified fluid. *Fluid Dyn.* **2007**, *42*, 255–267. [CrossRef]
64. Kistovich, A.V.; Chashechkin, Y.D. Dissipative-gravity waves in subcritical regimes of multicomponent convection. *Izv. Atmosph. Ocean. Phys.* **2001**, *37*, 476–481.
65. Allshouse, M.; Barad, M.; Peacock, T. Propulsion generated by diffusion-driven flow. *Nat. Phys.* **2010**, *6*, 516–519. [CrossRef]
66. Dimitrieva, N.F.; Chashechkin, Y.D. Fine structure of stratified flow around a fixed and slow moving wedge. *Oceanology* **2018**, *58*, 340–349. [CrossRef]
67. Levitsky, V.V.; Dimitrieva, N.F.; Chashechkin, Y.D. Visualization of the self-motion of a free wedge of neutral buoyancy in a tank filled with a continuously stratified fluid and calculation of perturbations of the fields of physical quantities putting the body in motion. *Fluid Dyn.* **2019**, *54*, 948–957. [CrossRef]
68. Makarov, S.A.; Chashechkin, Y.D. Coupled internal waves in a viscous incompressible fluid. *Izv. Atmos. Ocean. Phys.* **1982**, *18*, 758–764.
69. Sysoeva, E.Y.; Chashechkin, Y.D. Spatial structure of a wake behind a sphere in a stratified liquid. *J. Appl. Mech. Tech. Phys.* **1988**, *29*, 655–660. [CrossRef]
70. Sysoeva, E.Y.; Chashechkin, Y.D. Vortex structure of a wake behind a sphere in a stratified fluid. *J. Appl. Mech. Tech. Phys.* **1986**, *27*, 190–196. [CrossRef]
71. Chashechkin, Y.D. Conventional partial and new complete solutions of the fundamental equations of fluid mechanics in the problem of periodic internal waves with accompanying ligaments generation. *Mathematics* **2021**, *9*, 586. [CrossRef]
72. Sysoeva, E.Y.; Chashechkin, Y.D. Vortex systems in the stratified wake of a sphere. *Fluid Dyn.* **1991**, *26*, 544–551. [CrossRef]
73. Belyaev, V.S.; Savinkov, A.M.; Chashechkin, Y.D. Dynamics of laminar vortex rings in a stratified liquid. *J. Appl. Mech. Tech. Phys.* **1987**, *28*, 34–43. [CrossRef]
74. Turner, J.S. *Buoyancy Effects in Fluids*; CUP: Cambridge, UK, 1980; 412p.
75. Lin, Q.; Lindberg, W.R.; Boyer, D.L.; Fernando, H.J.S. Stratified flow past a sphere. *J. Fluid Mech.* **1992**, *240*, 315–354. [CrossRef]
76. Lin, Q.; Boyer, D.L.; Fernando, H.J.S. Turbulent wakes of linearly stratified flow past a sphere. *Phys. Fluids* **1992**, *4*, 1687–1696. [CrossRef]
77. Lin, Q.; Boyer, D.L.; Fernando, H.J.S. Internal waves generated by the turbulent wake of a sphere. *Exps. Fluids* **1993**, *15*, 147–154. [CrossRef]
78. Lin, Q.; Boyer, D.L.; Fernando, H.J.S. The vortex shedding of a stream-wise-oscillating sphere translating through a linearly stratified fluid. *Phys. Fluids* **1994**, *6*, 239–252. [CrossRef]

79. Hopfinger, E.J.; Flor, J.B.; Chomaz, J.M.; Bonneton, P. Internal waves generated by a moving sphere and its wake in a stratified fluid. *Exps. Fluids* **1991**, *11*, 255–261. [CrossRef]
80. Chomaz, J.-M.; Bonneton, P.; Butet, A.; Perrier, M.; Hopfinger, E.J. Froude number dependence of the flow separation line on a sphere towed in a stratified fluid. *Phys. Fluids A Fluid Dyn.* **1992**, *4*, 254–258. [CrossRef]
81. Chomaz, J.-M.; Bonneton, P.; Hopfinger, E.J. The structure of the near wake of a sphere moving horizontally in a stratified fluid. *J. Fluid Mech.* **1993**, *254*, 1–21. [CrossRef]
82. Bonnier, M.; Bonneton, P.; Eiff, O. Far-wake of a sphere in a stably stratified fluid: Characterization of the vortex structures. *Appl. Sci. Res.* **1998**, *59*, 269–281. [CrossRef]
83. Bonnier, M.; Eiff, O.; Bonnetone, P. On the density structure of far-wake vortices in a stratified fluid. *Dyn. Atm. Oceans* **2000**, *31*, 117–137. [CrossRef]
84. Bonneton, P.; Chomaz, J.; Hopfinger, E. Internal waves produced by the turbulent wake of a sphere moving horizontally in a stratified. *J. Fluid Mech.* **1993**, *254*, 23–40. [CrossRef]
85. Spedding, G.R.; Browand, F.K.; Fincham, A.M. Turbulence, similarity scaling and vortex geometry in the wake of a towed sphere in a stably stratified fluid. *J. Fluid Mech.* **1996**, *314*, 53–103. [CrossRef]
86. Meunier, P.; Diamessis, P.; Spedding, G.R. Self-preservation in stratified momentum wakes. *Phys. Fluids* **2006**, *18*, 106601. [CrossRef]
87. Voisin, B. Lee waves from a sphere in a stratified flow. *J. Fluid Mech.* **2007**, *574*, 273–315. [CrossRef]
88. Gushchin, V.A.; Matyushin, P.V. Vortex formation mechanisms in the wake behind a sphere for $200 < Re < 380$. *Fluid Dyn.* **2006**, *41*, 795–809. [CrossRef]
89. Gushchin, V.A.; Matyushin, P.V. Numerical simulation and visualization of vortical structure transformation in the flow past a sphere at an increasing degree of stratification. *Comput. Math. Math. Phys.* **2011**, *51*, 251–263. [CrossRef]
90. Gushchin, V.A.; Matyushin, P.V. Simulation and study of stratified flows around finite bodies. *Comput. Math. Math. Phys.* **2016**, *56*, 1034–1047. [CrossRef]
91. Orr, T.S.; Domaradzky, J.A.; Spedding, G.R.; Constantinescu, G.S. Numerical simulations of the near wake of a sphere moving in a steady, horizontal motion through a linearly stratified fluid at $Re = 1000$. *Phys. Fluids* **2015**, *27*, 035113. [CrossRef]